Tracking Innate Immune Activation in a Mouse Model of Parkinson's Disease Using TREM1 and TSPO PET Tracers

Katherine L. Lucot[1], Marc Y. Stevens[2], T. Adam Bonham[3], E. Carmen Azevedo[2], Aisling M. Chaney[2], Ebony D. Webber[3], Poorva Jain[2], Jessica L. Klockow[4], Isaac M. Jackson[2], Mackenzie L. Carlson[5], Edward E. Graves[4], Thomas J. Montine[1], and Michelle L. James[2,6]

[1]Department of Pathology, Stanford University, Stanford, California; [2]Department of Radiology, Molecular Imaging Program at Stanford, Stanford University, Stanford, California; [3]Department of Comparative Medicine, Stanford University, Stanford, California; [4]Department of Radiation Oncology, Molecular Imaging Program at Stanford, Stanford University, Stanford, California; [5]Department of Bioengineering, Stanford University, Stanford, California; and [6]Department of Neurology and Neurological Sciences, Stanford University, Stanford, California

Parkinson's disease (PD) is associated with aberrant innate immune responses, including microglial activation and infiltration of peripheral myeloid cells into the central nervous system (CNS). Methods to investigate innate immune activation in PD are limited and have not yet elucidated key interactions between neuroinflammation and peripheral inflammation. Translocator protein 18 kDa (TSPO) PET is a widely evaluated imaging approach for studying activated microglia and peripheral myeloid lineage cells in vivo but has yet to be fully explored in PD. Here, we investigate the utility of TSPO PET in addition to PET imaging of triggering receptor expressed on myeloid cells 1 (TREM1)—a novel biomarker of proinflammatory innate immune cells—for detecting innate immune responses in the 6-hydroxydopamine mouse model of dopaminergic neuron degeneration. **Methods:** C57/BL6J and *TREM1* knockout mice were stereotactically injected with 6-hydroxydopamine in the left striatum; control mice were injected with saline. At day 7 or 14 after surgery, mice were administered ^{18}F-GE-180, ^{64}Cu-TREM1 monoclonal antibody (mAb), or ^{64}Cu-isotype control mAb and imaged by PET/CT. Ex vivo autoradiography was performed to obtain high-resolution images of tracer binding within the brain. Immunohistochemistry was conducted to verify myeloid cell activation and dopaminergic cell death, and quantitative polymerase chain reaction and flow cytometry were completed to assess levels of target in the brain. **Results:** PET/CT images of both tracers showed elevated signal within the striatum of 6-hydroxydopamine–injected mice compared with those injected with saline. Autoradiography afforded higher-resolution brain images and revealed significant TSPO and TREM1 tracer binding within the ipsilateral striatum of 6-hydroxydopamine mice compared with saline mice at both 7 and 14 d after toxin. Interestingly, ^{18}F-GE-180 enabled detection of inflammation in the brain and peripheral tissues (blood and spleen) of 6-hydroxydopamine mice, whereas ^{64}Cu-TREM1 mAb appeared to be more sensitive and specific for detecting neuroinflammation, in particular infiltrating myeloid cells, in these mice, as demonstrated by flow cytometry findings and higher tracer binding signal-to-background ratios in brain. **Conclusion:** TSPO and TREM1 PET tracers are promising tools for investigating different cell types involved in innate immune activation in the context of dopaminergic neurodegeneration, thus warranting further investigation in other PD rodent models and human postmortem tissue to assess their clinical potential.

Received Aug. 16, 2021; revision accepted Feb. 10, 2022.

For correspondence or reprints, contact Michelle L. James (mljames@stanford.edu).

Published online Feb. 17, 2022.

Key Words: Parkinson's disease; neuroinflammation; molecular imaging; TSPO PET; TREM1 PET

J Nucl Med 2022; 63:1570–1578
DOI: 10.2967/jnumed.121.263039

Parkinson's disease (PD) is the most common movement disorder and the second most common neurodegenerative disease. Affecting nearly 7 million people worldwide (*1–3*), PD encompasses a wide spectrum of motor, cognitive, autonomic, and psychiatric symptoms. PD is characterized pathologically by dopaminergic neuron loss in the substantia nigra and accumulation of Lewy bodies and neurites, which contain misfolded α-synuclein protein, within neurons. Neuroinflammation is intimately tied to both dopaminergic neuron loss and α-synuclein accumulation, indicating this to be an early event in PD pathogenesis (*4*). Activated microglial cells, peripheral myeloid-mediated proinflammatory innate immune responses, and neurotoxic adaptive immune activity in the central nervous system (CNS) are also specifically involved in PD pathogenesis (*5,6*).

Methods to investigate inflammatory processes in PD brain are restricted mainly to postmortem tissue or cerebrospinal fluid. Although these studies have yielded useful insights on the presence of activated microglia and altered proinflammatory cytokine concentrations in the substantia nigra and cerebrospinal fluid of PD patients (*7–15*), they are often obtained at a single time point and are therefore limited in the information they can provide on highly dynamic immune responses.

PET imaging of translocator protein 18 kDa (TSPO)—an established imaging biomarker of inflammation, predominately upregulated in activated microglia and peripheral myeloid lineage cells (e.g., macrophages, monocytes, and neutrophils)—is a useful method to visualize neuroinflammation in living subjects. ^{18}F-GE-180 is one of the most sensitive and specific TSPO PET tracers for imaging rodent models of neuroinflammation (*16–20*) because of its high signal-to-background ratio as demonstrated through head-to-head comparison studies with ^{18}F-PBR06 (*19*), ^{11}C-(*R*)-PK11195 (*20*), and ^{18}F-DPA-714 (*21*); however, it has not yet been evaluated in PD mouse models (*22,23*). Additionally, triggering receptor expressed on myeloid cells 1 (TREM1) (*24*) was recently identified as a novel, highly specific imaging biomarker of proinflammatory innate immune cells: our laboratory reported the first TREM1 PET tracer, ^{64}Cu-TREM1

monoclonal antibody (mAb), and demonstrated its ability to detect peripheral CNS-infiltrating TREM1-positive myeloid cells in mouse models of stroke and multiple sclerosis (2.5–3.5 percentage injected dose per gram in brain regions of interest) (*25–27*).

Here, we set out to assess the potential of these 2 promising PET imaging biomarkers for providing unique insights into the spatiotemporal dynamics of innate immune responses in the context of PD and neuroinflammation. We hypothesized that detection of TSPO and TREM1 PET by ^{18}F-GE-180 and ^{64}Cu-TREM1 mAb, respectively, can track different aspects of innate immune activation in a mouse model of dopaminergic neurodegeneration.

MATERIALS AND METHODS

Study Design

6-Hydroxydopamine hydrobromide (6-hydroxydopamine) selectively damages dopaminergic neurons and protracts degeneration of the nigrostriatal system when injected into the striatum unilaterally (*28*). We performed TSPO and TREM1 PET imaging 7 and 14 d after intrastriatal injection of 6-hydroxydopamine or vehicle (saline). TSPO and TREM1 tracer specificity was assessed using PK-11195, a TSPO ligand, and an appropriate isotype control antibody, respectively. Since the unlabeled TREM1 tracer and other available TREM1 antibodies are agonists, they cannot be used for mass-level blocking experiments without perturbing the molecular pathways of interest in our mouse model; therefore, *TREM1* knockout mice were imaged 7 d after 6-hydroxydopamine injection to further assess specificity of the TREM1 PET agent. Binding and spatial distribution of each tracer were confirmed by ex vivo γ-counting and high-resolution autoradiography. Alterations in immune activation were confirmed using flow cytometry, immunohistochemistry, and reverse-transcription quantitative polymerase chain reaction (PCR). Figure 1 summarizes the study time line, and Supplemental Table 1 shows the numbers of mice and tissue samples used for each experiment (supplemental materials are available at http://jnm.snmjournals.org).

Animals

All experiments involving animals were completed in accordance with the Stanford Administrative Panel on Laboratory Animal Care, which is accredited by the Association for the Assessment and Accreditation of Laboratory Animal Care International. Male 8- to 12-wk-old C57BL/6J wild-type mice (Jackson Laboratories) and *TREM1* knockout littermates (*29*), a kind gift from the laboratory of Professor Katrin Andreasson (Stanford University, original breeders provided by Dr. Christoph Mueller, University of Bern), were housed in a temperature-controlled environment under a 12-h light/dark schedule with unrestricted access to food and water. When indicated, anesthetization was performed using isoflurane.

6-Hydroxydopamine Model Induction

6-Hydroxydopamine (10 μg/μL; Sigma) or saline was injected (1 μL) into the striatum of anesthetized mice during stereotactic surgery (coordinates: anterior/posterior = 0.5, lateral = 1.8, dorsal/ventral = −3.5) using established methods (*30,31*).

^{18}F-GE-180 Radiolabeling

^{18}F-GE-180 was radiosynthesized according to standard methods (*22*). The tracer was formulated in phosphate-buffered saline (0.1 M NaCl, 0.05 M sodium phosphate, pH 7.4) containing 10% ethanol. A molar activity of 44.4 GBq/μmol and high radiochemical purity (>95%) were achieved.

TREM1 DOTA Conjugation

Mouse TREM1 mAb (R&D Systems) was conjugated with DOTA-*N*-hydroxysuccinimide (Macrocyclics) using metal-free buffers and previously published procedures (*25,32*). The average number of chelator molecules per antibody was determined to be 0.8–1.9 using electrospray ionization mass spectrometry and matrix-assisted laser desorption/ionization time of flight. The average was determined after performing 3 independent reactions.

^{64}Cu-TREM1 mAb and Isotype Control Radiolabeling

TREM1 mAb and isotype control mAb were radiolabeled using previously reported general copper-labeling methods (*25,33,34*). Briefly, immunoconjugate (80 ± 11 μg, n = 4) in NH_4OAc (pH 5.5) was added to $^{64}CuCl_2$ (0.06 GBq) in NH_4OAc under gentle agitation at 37°C. The reaction was monitored via radio–thin-layer chromatography until a labeling efficiency of more than 99% was observed (15–30 min), at which point 2 μL of ethylenediaminetetraacetic acid (50 mM) were added. Reactions were analyzed by radio–thin-layer chromatography and size-exclusion high-performance liquid chromatography (Phenomenex 00H-2146-K0, 5 μm SEC-s3000 400 Å, 300 × 7.8 mm). Pure fractions (>99%) of ^{64}Cu-TREM1 mAb and isotype control mAb were combined and diluted with saline. The molar activity of each tracer was determined to be more than 70 GBq/μmol, and high radiochemical purity (>97%) was achieved.

In Vivo PET/CT Acquisition

Mice were imaged using a dual small-animal PET/CT scanner (GNEXT; Sophie) 7 or 14 d after stereotactic injection of 6-hydroxydopamine. Isotype control, blocking, *TREM1* knockout, and saline studies were conducted on day 7. Mice were anesthetized and intravenously injected (3.7–5.55 MBq) with their respective tracer (Supplemental Table 1).

CT images were acquired as previously described (*35*) for anatomic reference before a 10-min static PET acquisition 50 min after administration of ^{18}F-GE-180 or 19 h after intravenous injection of ^{64}Cu-TREM1 mAb or ^{64}Cu-isotype control mAb. A calibration factor was calculated each imaging day on the basis of a reference standard consisting of a 20-mL syringe containing a known amount of ^{18}F or ^{64}Cu. PET data were acquired and reconstructed as previously described by our laboratory (*25*).

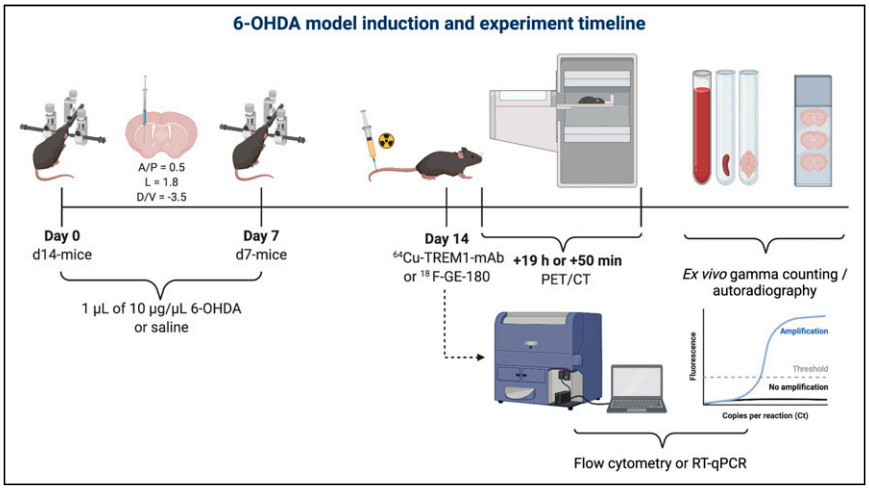

FIGURE 1. Study design of 6-hydroxydopamine model induction and imaging time line. d7- and d14-mice refer to mice injected with 6-hydroxydopamine or saline 7 or 14 d, respectively, before imaging or flow cytometry. A/P = anterior/posterior; D/V = dorsal/ventral; L = lateral; OHDA = hydroxydopamine; RT-qPCR = reverse transcription-quantitative polymerase chain reaction.

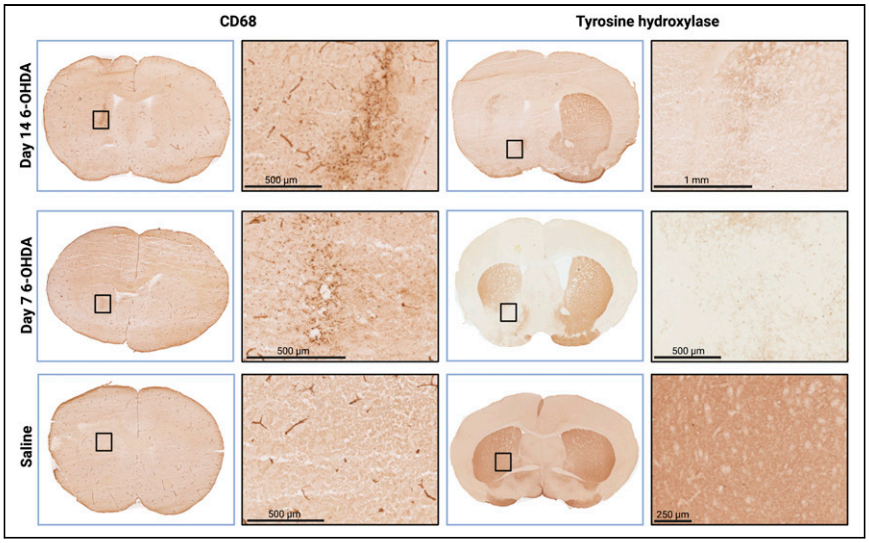

FIGURE 2. Immunohistochemistry of representative mouse brains injected with either 6-hydroxydopamine or saline. (Left) CD68 immunohistochemistry in brains of 6-hydroxydopamine or saline mice, with zoomed images beside their respective coronal brain images. CD68-positive immunostaining was present in slightly different regions of brain because of small variations in injection site. (Right) Tyrosine hydroxylase staining of dopaminergic processes in ipsilateral and contralateral striata of mice injected with 6-hydroxydopamine or saline. Ice crystals, or bubbles (freezing artifacts), due to rapid freezing can be seen in zoomed images. OHDA = hydroxydopamine.

PET Analysis and Quantitation

PET and CT images were coregistered and analyzed using VivoQuant (version 4.0; inviCRO) and Inveon Research Workspace software (Siemens) to quantify tracer uptake in specific regions of interest. For striatum quantitation, a 3-dimensional mouse brain atlas was fit to the PET/CT images via alignment of the atlas with the skull of each mouse (as determined by CT).

^{18}F-GE-180 Blocking Studies

Blocking studies were conducted 7 d after stereotactic 6-hydroxydopamine injection. The TSPO ligand PK-11195 (3 mg/kg; Sigma-Aldrich) was administered intravenously 15 min before ^{18}F-GE-180 injection, and a subsequent 10-min static PET scan was acquired at 50–60 min after tracer injection.

γ-Counting and Autoradiography

On scan completion, cardiac puncture was performed under anesthesia, and the mice were subsequently perfused with 30 mL of phosphate-buffered saline, pH 7.4 (1 time), to assess tracer uptake and spatial distribution in tissues while eliminating the contribution of tracer signal in blood. Brain, blood, and spleen were harvested, weighed, and counted using an automatic γ-counter (Hidex). Brains were immediately submerged in phosphate-buffered saline before being counted to reduce the likelihood of drying before subsequent freezing for ex vivo autoradiography. Percentage injected dose per gram was calculated for each organ of interest. Immediately after γ-counting, brains were frozen in optimal-cutting-temperature compound, and 40-μm-thick sections were cut for autoradiography (Microm HM550 Microtome; Leica Biosystems) and exposed to digital films for a minimum of 10 half-lives. Films were scanned using a Typhoon phosphor scanner (Cytiva), and the mean pixel intensity in the ipsilateral versus contralateral striatum was quantified using Image J (version 1.53a).

Immunohistochemistry

The same brain sections as used for autoradiography were probed with antibodies to CD68 (marker for microglia and other myeloid lineage cells) and tyrosine hydroxylase (marker for dopaminergic cells) using standard procedures (*36*).

Briefly, sections were fixed in acetone for 10 min, thoroughly washed in tris-buffered saline, and pretreated with 0.6% H_2O_2 in 0.3% Triton X (Union Carbide)–tris-buffered saline before overnight 4°C incubation with anti-CD68 (rat, 1:500; Bio Rad) and anti–tyrosine hydroxylase (rabbit, 1:3,000; Abcam) antibodies. The following day, sections were washed with tris-buffered saline, incubated for 1 h with ImmPRESS horseradish peroxidase antirat IgG polymer detection kit (Vector Laboratories) and ImmPRESS horse antirabbit IgG PLUS polymer kit (Vector Laboratories), and subsequently exposed to 0.05% 3,3-diaminobenzidine (Sigma-Aldrich) in 0.1 M TrisHCl (pH 7.4) with 0.03% H_2O_2 for 1–3 min. Sections were washed with 0.1 M TrisHCl before application of a coverslip. Images were captured using a Nanozoomer 2.0-RS (Hamamatsu).

RNA Isolation and Gene Expression Analysis

Ipsilateral brain sections were harvested from anesthetized mice after perfusion, immediately flash-frozen in TRIzol (Invitrogen), and stored at −80°C until use. RNA was extracted

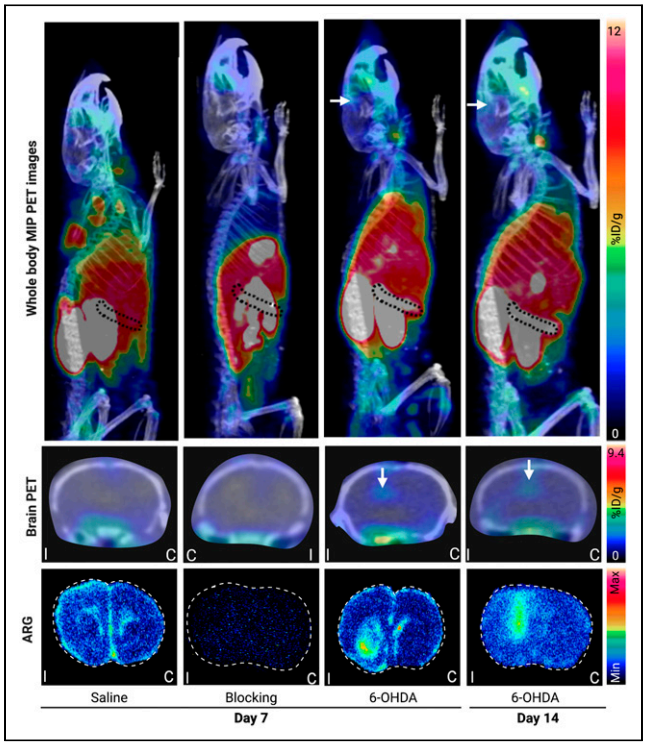

FIGURE 3. Representative ^{18}F-GE-180 PET/CT whole-body maximum-intensity-projection images, coronal brain images, and autoradiography of 40-μm-thick coronal mouse brain sections. Black and white dashed outlines indicate spleen and coronal brain sections, respectively. Arrows point to areas of increased TSPO PET signal around site of 6-hydroxydopamine injection. %ID = percentage injected dose; ARG = autoradiography; C = contralateral brain hemisphere; I = ipsilateral brain hemisphere; MIP = maximum-intensity projection; OHDA = hydroxydopamine.

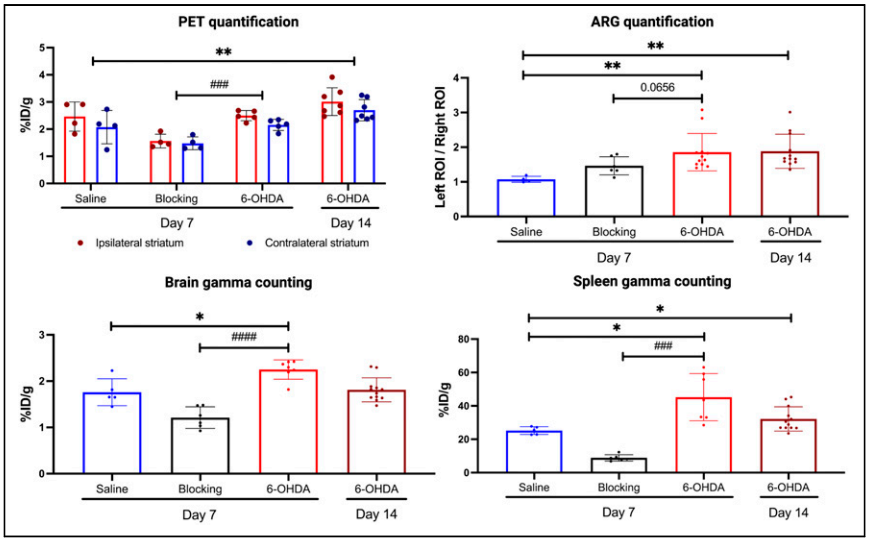

FIGURE 4. Quantification of TSPO PET tracer signal (saline ipsilateral, 2.5 ± 0.53; saline contralateral, 2.1 ± 0.61; blocking ipsilateral, 1.6 ± 0.25; blocking contralateral, 1.5 ± 0.24; day 7 6-hydroxydopamine ipsilateral, 2.5 ± 0.19; day 7 6-hydroxydopamine contralateral, 2.2 ± 0.20; day 14 6-hydroxydopamine ipsilateral, 3.0 ± 0.51; day 14 6-hydroxydopamine contralateral, 2.7 ± 0.39), ex vivo autoradiography (saline, 1.1 ± 0.09; blocking, 1.5 ± 0.26; day 7 6-hydroxydopamine, 1.9 ± 0.49; day 14 6-hydroxydopamine, 1.9 ± 0.54), and γ-counting quantification (brain: saline, 1.8 ± 0.29; blocking, 1.2 ± 0.23; day 7 6-hydroxydopamine, 2.3 ± 0.21; day 14 6-hydroxydopamine, 1.8 ± 0.26; spleen: saline, 25.2 ± 2.33; blocking, 8.9 ± 1.89; day 7 6-hydroxydopamine, 45.2 ± 14.13; day 14 6-hydroxydopamine, 32.2 ± 7.26) in saline, blocking, and 6-hydroxydopamine mice. All groups were compared with saline control (significance denoted by *); day 7 6-hydroxydopamine and blocking were compared (significance denoted by #). Data are mean ± SD percentage injected dose per gram. $^{*}P < 0.05$. $^{**}P < 0.01$. $^{\#\#\#}P < 0.001$. $^{\#\#\#\#}P < 0.0001$. %ID = percentage injected dose; ARG = autoradiography; OHDA = hydroxydopamine; ROI = region of interest.

following the TRIzol reagent RNA isolation standard operating procedure (Invitrogen). Briefly, tissues were homogenized, and RNA was isolated using chloroform (Sigma-Aldrich). Messenger RNA was precipitated and then purified in isopropanol and 75% EtOH, and the product was suspended in nuclease-free water. All messenger RNA was assessed for concentration and quality using an Eppendorf BioSpectrometer.

Complementary DNA was synthesized using the RT^2 First Strand kit (Qiagen), and incubation steps were completed in the Thermal Cycler Mini Amp (Applied Biosystems), per kit protocol. PCR was performed with SYBR green polymerase (Qiagen), reverse-transcription PCR Qiagen-specified primers (*TSPO, TREM1,* and *GAPDH*), and complementary DNA. *GAPDH* was used as a housekeeping gene. Reactions were completed in the Applied Biosystems QuantStudio 6 Real-Time PCR machine. Each sample was run with 3 technical replicates, and fold-change for each gene was calculated by deriving $2^{\Delta\Delta CT}$. Transcripts with undetectable values were assigned a cycle threshold of 38 for analysis (*37*). Samples with high variation between technical replicates (SD > 0.70) were excluded from analysis.

Flow Cytometry

Day 7 6-hydroxydopamine and saline mice were perfused, and brains (ipsilateral and contralateral hemispheres) and spleens were harvested and processed into single-cell suspensions for flow cytometric analysis. Briefly, brain and spleen tissues were mechanically homogenized in CNS buffer (2.5% HEPES [2-[4-(2-hydroxyethyl)piperazin-1-yl]ethanesulfonic acid], pH 7.5 [Invitrogen] in Hanks balanced salt solution without calcium or magnesium [Gibco]) and fluorescent activated cell sorting buffer (2% fetal bovine serum in phosphate-buffered saline), respectively. Myelin was removed from brain samples using a Percoll (GE Healthcare) gradient (25% Percoll in CNS buffer). Resulting single-cell suspensions were stained for live/dead (Aqua; ThermoFisher Scientific), TREM1 (APC; R&D Systems), CD11c (PAC-Blue; Biolegend), Ly-6G (PE-Cy7; Biolegend), CD11b (APC-Cy7; Biolegend), CD3 (PE; Biolegend), and CD45 (PerCP-Cy5.5; Biolegend) to isolate immune cell populations. Cells were fixed in 2% paraformaldehyde (Santa Cruz Biotechnology) before analysis. Data were gated (Supplemental Fig. 1) and analyzed using FlowJo (version 10.7.1).

Statistics

Statistical analyses were performed using GraphPad Prism (version 9.1.1). Data were assessed for normalization, and parametric/nonparametric tests were applied as appropriate before 2-way (PET and flow cytometry) or 1-way (autoradiography, γ-counting, and gene expression) ANOVA. *P* values of less than 0.05 were considered statistically significant.

RESULTS

Injection of 6-Hydroxydopamine Induces Dopaminergic Neurodegeneration and Myeloid Cell Activation

To confirm dopaminergic neurodegeneration and immune response in our PD rodent model, immunohistochemistry was performed on brain slices 7 and 14 d after striatal injection of 6-hydroxydopamine or saline, at which time activation of microglial/macrophages and dopaminergic cell loss is expected to be greatest (*38*). CD68 immunohistochemistry of striatum showed activated microglia/macrophages in and around the site of toxin injection (Fig. 2; Supplemental Fig. 2). Importantly, this marker did not detect significant levels of activated microglia/macrophages in the saline mice, indicating that the immune activation was specific to 6-hydroxydopamine injection. Tyrosine hydroxylase immunohistochemistry confirmed both the loss of dopaminergic processes at the toxin injection site and the presence of intact cells in the saline mice (Fig. 2). Unfortunately, accurate quantitation of our immunostaining was not possible because of the presence of freezing artifacts. These artifacts arose due to staining of the same tissue as used for autoradiography, which was not able to undergo extensive fixation protocols (i.e., sectioning and exposure to autoradiography films was performed 30–60 min after removal of brain tissue to minimize radioactive decay). Importantly, immunostaining of the same tissues as used for autoradiography enabled accurate quantitation of tracer signal in autoradiography images and provided clear, qualitative evidence of innate immune activation associated with dopaminergic cell loss, which appeared to be more pronounced 14 d after 6-hydroxydopamine, aligning with the results from a similar study performed by Cicchetti et al. (Fig. 2; Supplemental Fig. 2) (*38*).

TSPO PET Imaging Enables Visualization of Innate Immune Activation in Brain, Spleen, and Blood of 6-Hydroxydopamine–Injected Mice

To investigate the ability of TSPO PET to detect innate immune activation in the 6-hydroxydopamine model, in vivo PET images were acquired at 50–60 min after injection of ^{18}F-GE-180 (Fig. 3; Supplemental Fig. 3). Whole-body images revealed increased tracer uptake in the brains of day 7 and day 14 6-hydroxydopamine mice

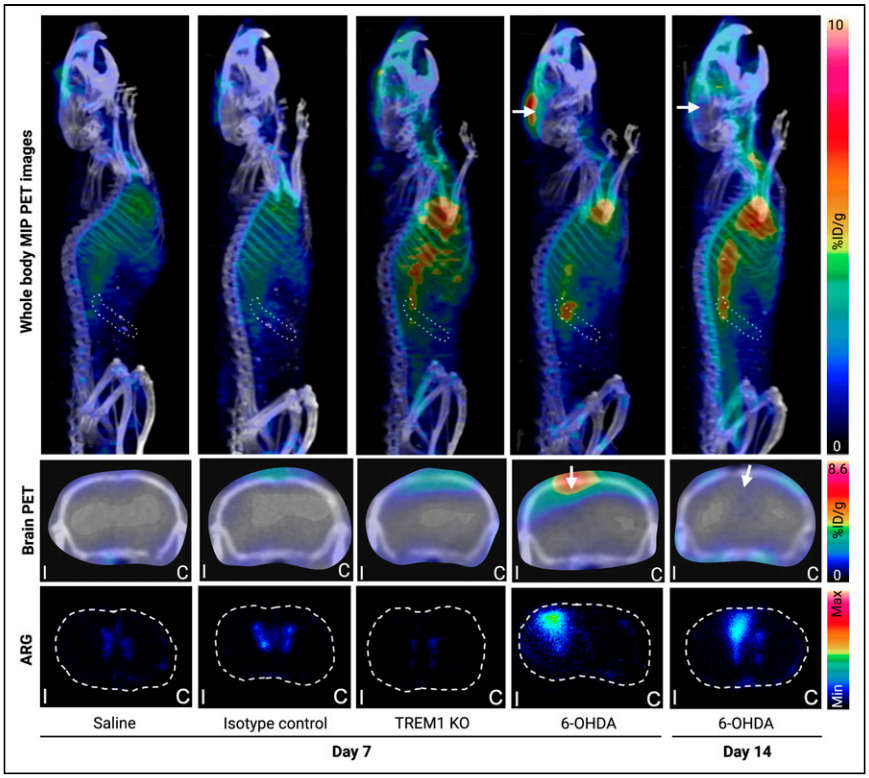

FIGURE 5. Representative ^{64}Cu-TREM1 PET/CT whole-body maximum-intensity-projection images, coronal brain images, and autoradiography of 40-μm-thick coronal mouse brain sections. Dashed outlines indicate spleen and coronal brain sections. %ID = percentage injected dose; ARG = autoradiography; C = contralateral brain hemisphere; I = ipsilateral brain hemisphere; KO = knockout; MIP = maximum-intensity projection; OHDA = hydroxydopamine.

compared with saline mice and day 7 6-hydroxydopamine mice pretreated with PK1119. In the periphery, we observed increased signal in adipose tissue (brown and white), kidneys, spleen, liver, and lungs (all tissues known to express TSPO (*39*)) of day 7 and day 14 6-hydroxydopamine mice, whereas, preblocked mice contained signal only in the gastrointestinal tract (indicative of tracer excretion), thus proving the specificity of ^{18}F-GE-180 in this model. PET signal was quantified in the ipsilateral and contralateral striata (Fig. 4). Quantitation of PET images confirmed there was a significant increase in tracer binding in the ipsilateral striatum of day 14 6-hydroxydopamine mice compared with saline mice ($P < 0.01$), in addition to significant attenuation of signal in 6-hydroxydopamine–injected mice preblocked with PK-11195 ($P < 0.001$), confirming tracer specificity.

Ex vivo autoradiography of both day 7 and day 14 6-hydroxydopamine mouse brains exhibited significantly elevated tracer binding compared with saline mice ($P < 0.01$), with striatal tracer uptake ratios (ipsilateral to contralateral striatum) determined to be 1.9 for day 7 6-hydroxydopamine, 1.9 for day 14 6-hydroxydopamine, 1.1 for saline, and 1.5 for blocking mice (Figs. 3 and 4). γ-counting of whole brain, spleen, and peripheral blood (Fig. 4; Supplemental Fig. 4A) revealed significantly increased tracer uptake in all 3 tissues of day 7 6-hydroxydopamine mice ($P < 0.05$ for all 3 tissues). Day 14 6-hydroxydopamine mice showed a significant difference only in spleen ($P < 0.05$), when compared with saline animals. Importantly, γ-counting of brain tissue was performed using whole-brain tissue (as opposed to ipsilateral vs. contralateral hemisphere), which could have diluted the differences in signal observed in injured versus uninjured striata within autoradiography images. PK-11195 blocking significantly decreased tracer uptake in the brain ($P < 0.0001$) and spleen ($P < 0.001$) of day 7 6-hydroxydopamine mice. The increased TSPO PET and autoradiography signal was supported by reverse-transcription quantitative PCR findings, which revealed a strong trend that ipsilateral striatal *TSPO* messenger RNA levels trended toward significance in day 7 6-hydroxydopamine mice ($P < 0.0598$) and were significantly increased in day 14 6-hydroxydopamine mice ($P < 0.01$, Supplemental Fig. 5A). Taken together, these data indicate that TSPO PET shows promise for visualizing inflammation in the brain, spleen, and blood of this rodent model of dopaminergic degeneration.

TREM1 Imaging Reveals Infiltrating Innate Immune Cells in the Brain of 6-Hydroxydopamine–Injected Mice

To assess the ability of TREM1 PET to detect activated myeloid cells in 6-hydroxydopamine mice, whole-body PET/CT images were acquired (Fig. 5; Supplemental Fig. 6) and signal quantified in the ipsilateral versus contralateral striatum (Fig. 6). Whole-body images showed that in the spleen, signal was higher in day 7 and day 14 6-hydroxydopamine mice than in isotype control, knockout, and saline mice. There also appeared to be higher blood signal in day 7 and day 14 6-hydroxydopamine mice (in addition to knockout mice) than in isotype control and saline mice. Quantitation of PET data confirmed that day 7 6-hydroxydopamine mice had significantly higher tracer binding in the ipsilateral striatum than did isotype control injected mice ($P < 0.01$). Though not statistically significant, PET quantitation trended toward higher tracer binding in the striatum of day 7 6-hydroxydopamine mice than in saline controls ($P < 0.08$). Of note, TREM1 PET signal in the ipsilateral striata of knockout mice was not significantly different from that in wild-type mice 7 d after 6-hydroxydopamine injection ($P < 0.32$), most likely due to the presence of unbound tracer residing in the blood of knockout mice since they lack TREM1 (and thus more tracer remains in the blood pool as opposed to binding to target-containing tissues). In particular, there appeared to be elevated signal in the cortex of knockout mice close to the surgical site, where a hole was drilled to allow injection of 6-hydroxydopamine. After removal of unbound tracer in blood via perfusion, brain tissues were further evaluated using ex vivo autoradiography (Figs. 5 and 6). Autoradiography showed that TREM1 tracer binding was significantly elevated in the injured brain tissue of day 7 ($P < 0.05$) and day 14 ($P < 0.01$) 6-hydroxydopamine mice compared with saline mice. Importantly, day 7 6-hydroxydopamine mice had significantly increased tracer binding compared with the knockout mice ($P < 0.01$), and knockout mouse brains no longer contained any signal, confirming tracer specificity. Ratios of autoradiography signal in the injured to uninjured brain were as follows: 2.2 for day 7 6-hydroxydopamine, 3.3 for day 14 6-hydroxydopamine, 1.1 for saline, 1.7 for isotype control, and 1.0 for *TREM1* knockout mice.

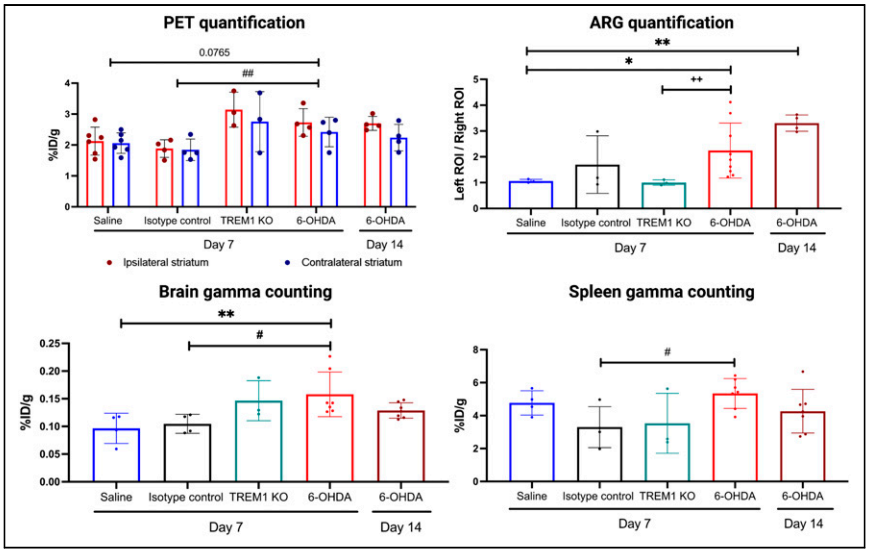

FIGURE 6. Quantification of TREM1 PET tracer signal (saline ipsilateral, 2.1 ± 0.45; saline contralateral, 2.1 ± 0.33; isotype control ipsilateral, 1.9 ± 0.29; isotype control contralateral, 1.8 ± 0.35; *TREM1* knockout ipsilateral, 3.1 ± 0.57; *TREM1* knockout contralateral, 2.8 ± 0.97; day 7 6-hydroxydopamine ipsilateral, 2.7 ± 0.45; day 7 6-hydroxydopamine contralateral, 2.4 ± 0.48; day 14 6-hydroxydopamine ipsilateral, 2.7 ± 0.23; day 14 6-hydroxydopamine contralateral, 2.2 ± 0.43), ex vivo autoradiography (saline, 1.1 ± 0.07; isotype control, 1.7 ± 1.12; *TREM1* knockout, 1.0 ± 0.17; day 7 6-hydroxydopamine, 2.2 ± 1.07; day 14 6-hydroxydopamine, 3.3 ± 0.32), and γ-counting quantification (brain: saline, 0.1 ± 0.03; isotype control, 0.1 ± 0.02; *TREM1* knockout, 0.15 ± 0.04; day 7 6-hydroxydopamine, 0.16 ± 0.04; day 14 6-hydroxydopamine, 0.13 ± 0.01; spleen: saline, 4.8 ± 0.74; isotype control, 3.3 ± 1.2; *TREM1* knockout, 3.5 ± 1.82; day 7 6-hydroxydopamine, 5.4 ± 0.91; day 14 6-hydroxydopamine, 4.3 ± 1.32) in saline, isotype control, and 6-hydroxydopamine mice. All groups were compared with saline control (significance denoted by *); day 7 6-hydroxydopamine and isotype control were compared (significance denoted by #) as well as day 7 6-hydroxydopamine and *TREM1* knockout (significance denoted by +). Data are mean ± SD percentage injected dose per gram. $^{*/\#}P < 0.05$. $^{**/\#\#/++}P < 0.01$. %ID = percentage injected dose; ARG = autoradiography; KO = knockout; OHDA = hydroxydopamine; ROI = region of interest.

Ex vivo γ-counting was performed on whole brain, spleen, and peripheral blood (from cardiac puncture; Fig. 6; Supplemental Fig. 4B). Tracer binding was significantly increased in the whole brain of day 7 6-hydroxydopamine mice ($P < 0.01$) and trended higher in the peripheral blood of day 14 6-hydroxydopamine mice ($P < 0.13$) than in saline mice. Additionally, tracer signal was significantly increased in all organs of day 7 6-hydroxydopamine mice compared with isotype control ($P < 0.01$ for brain and < 0.05 for spleen and blood). Reverse-transcription quantitative PCR analysis revealed that *TREM1* expression was markedly increased in day 14 6-hydroxydopamine mice ($P < 0.05$), whereas increases in day 7 6-hydroxydopamine mice trended toward significance ($P < 0.08$, Supplemental Fig. 4B).

To confirm the presence of TREM1-positive immune cells after dopaminergic neuron damage, flow cytometry was performed on ipsilateral and contralateral brain regions (Fig. 7). A significant increase in the infiltration (expressed as percentage live singlets) of peripheral myeloid ($CD45^{hi}$ [hi = high] CD11b-positive) cells was observed in the ipsilateral hemisphere of day 7 6-hydroxydopamine mice compared with the contralateral hemisphere of day 7 6-hydroxydopamine mice ($P < 0.0001$) and the ipsilateral hemisphere of saline mice ($P < 0.001$, Fig. 7A). Increased lymphoid (CD45-positive CD11b-negative) cell infiltration was also observed in the ipsilateral versus contralateral region of day 7 6-hydroxydopamine mice ($P < 0.0001$). In contrast, microglia populations ($CD45^{int}$ [int= intermediate] CD11b-positive) were unchanged by 6-hydroxydopamine treatment. No significant changes in myeloid or lymphoid cell populations were observed in the spleens of day 7 6-hydroxydopamine or saline mice (Supplemental Fig. 7). Phenotyping of immune cell subtypes revealed significantly elevated TREM1-positive myeloid cells in the ipsilateral brain of day 7 6-hydroxydopamine mice (vs. contralateral in day 7 6-hydroxydopamine mice [$P < 0.0001$] and ipsilateral in saline mice [$P = 0.01$], Fig. 7B). TREM1 expression was not observed on infiltrating lymphoid cells and did not significantly change on microglial cells, confirming that the increased signal observed in PET and autoradiography images is due primarily to infiltration of TREM1-positive peripheral myeloid lineage cells.

Further characterization of infiltrating myeloid cells revealed an increased frequency of neutrophils ($CD45^{hi}$ CD11b-positive Ly6G-positive) compared with monocyte/macrophage/dendritic cells ($CD45^{hi}$ CD11b-positive Ly6G-negative) (Supplemental Fig. 8A). A large number of neutrophils compared with monocytes/macrophages/dendritic cells were found to infiltrate the ipsilateral brain of day 7 6-hydroxydopamine mice ($P < 0.001$). Moreover, a higher frequency of neutrophils were TREM1-positive ($P < 0.01$, Supplemental Fig. 8B), suggesting that most TREM1 PET signal observed after 6-hydroxydopamine treatment represents TREM1-positive neutrophils. Together, these data indicate that TREM1 PET is a highly specific approach for visualizing the presence of early proinflammatory innate immune activation in the 6-hydroxydopamine model of dopaminergic neurodegeneration.

DISCUSSION

The utility of ^{18}F-GE-180 and ^{64}Cu-TREM1 mAb to enable quantification of whole-body innate immune responses was evaluated in the 6-hydroxydopamine mouse model. We understand that PD is a highly complex chronic, progressive neurodegenerative disorder and that there is no mouse model that recapitulates this disease. Importantly, the rodent model we chose has been extensively studied and is known to contain selective dopaminergic degeneration in addition to innate immune activation, making it a suitable starting point to study the ability of TREM1 and TSPO PET to detect activated myeloid cells in the context of PD pathology (*30*). Better understanding the inflammatory responses in PD may enable more accurate monitoring of disease progression and response to novel therapies and, ultimately, help to prevent or reset the chronic neuroinflammation that exacerbates disease (*40*).

Here, we have shown that TSPO and TREM1 tracers enabled detection of complementary molecular information in the 6-hydroxydopamine mouse model through detecting 2 distinct immune cell types involved in innate immune responses associated with dopaminergic degeneration. Because of the current limitations of small-animal PET (i.e., relatively low spatial resolution and the partial-volume effect), our in vivo imaging data were

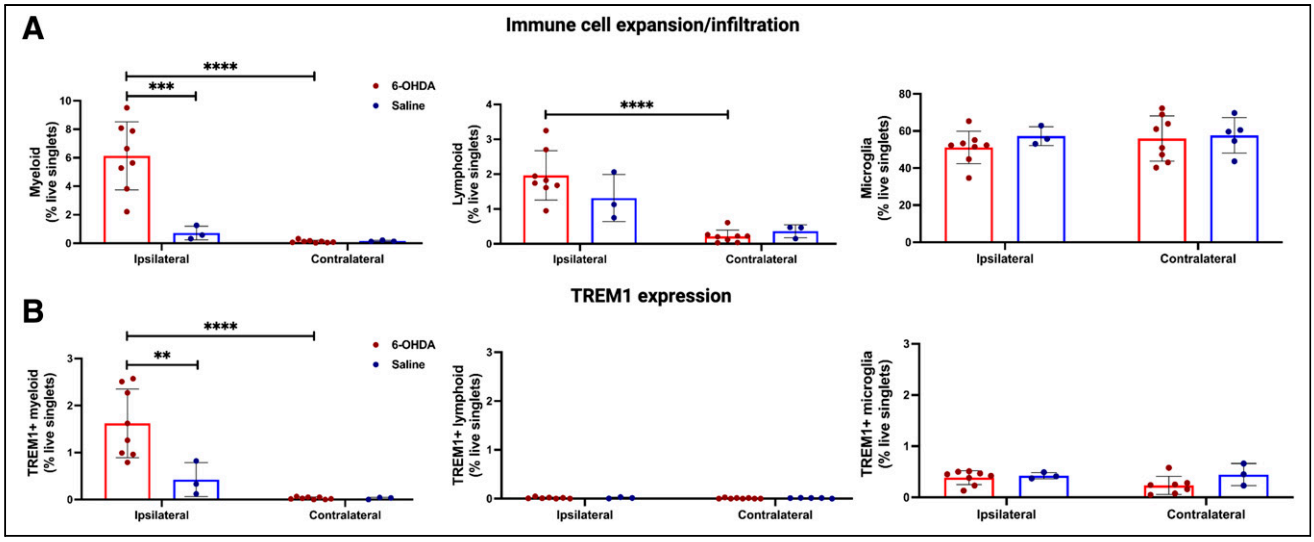

FIGURE 7. Flow cytometry analysis of 6-hydroxydopamine and saline brains. (A) Flow cytometry analysis demonstrating frequency of peripheral myeloid ($CD45^{hi}$ [hi = high] CD11b-positive), lymphoid (CD45-positive CD11b-negative), and microglial ($CD45^{int}$ [int= intermediate] CD11b-positive) cells in brains of 6-hydroxydopamine and saline mice 7 d after stereotactic injection (myeloid: day 7 6-hydroxydopamine ipsilateral, 6.1 ± 0.72; day 7 6-hydroxydopamine contralateral, 0.12 ± 0.09; saline ipsilateral, 0.72 ± 0.48; saline contralateral, 0.16 ± 0.05; lymphoid: day 7 6-hydroxydopamine ipsilateral, 2.0 ± 0.71; day 7 6-hydroxydopamine contralateral, 0.21 ± 0.18; saline ipsilateral, 1.3 ± 0.67; saline contralateral, 0.36 ± 0.18; microglia: day 7 6-hydroxydopamine ipsilateral, 51.1 ± 8.76; day 7 6-hydroxydopamine contralateral, 55.9 ± 12.18; saline ipsilateral, 57.2 ± 5.12; saline contralateral, 57.6 ± 9.54). (B) Frequency of TREM1-positive myeloid, lymphoid, and microglial cells (TREM1-positive myeloid: day 7 6-hydroxydopamine ipsilateral, 1.6 ± 0.73; day 7 6-hydroxydopamine contralateral, 0.03 ± 0.025; saline ipsilateral, 0.42 ± 0.36; saline contralateral, 0.026 ± 0.023; TREM1-positive lymphoid: day 7 6-hydroxydopamine ipsilateral, 0.014 ± 0.016; day 7 6-hydroxydopamine contralateral, 0.0068 ± 0.01; saline ipsilateral, 0.016 ± 0.014; saline contralateral, 0.011 ± 0.0065; TREM1-positive microglia: day 7 6-hydroxydopamine ipsilateral, 0.39 ± 0.14; day 7 6-hydroxydopamine contralateral, 0.23 ± 0.18; saline ipsilateral, 0.42 ± 0.061; saline contralateral, 0.45 ± 0.22). Data are mean ± SD percentage total live singlets. $^{**}P < 0.01$. $^{***}P < 0.001$. $^{****}P < 0.0001$. OHDA = hydroxydopamine.

corroborated by additional ex vivo methods. Specifically, we performed high-resolution ex vivo autoradiography together with immunostaining of the same tissue slices and confirmed the specific correspondence of ^{18}F-GE180 and ^{64}Cu-TREM1 mAb binding in regions containing activated myeloid cells in 6-hydroxydopamine mice. Importantly, we did not observe the exact same results using γ-counting since we used whole brain as opposed to ipsilateral versus contralateral brain tissue, which likely dilutes the differences found using autoradiography. Since autoradiography affords high-resolution images depicting spatial distribution and binding of tracers, it permits more accurate quantitation. Thus, the results from our autoradiography analyses more reliably represent the extent of tracer binding and its correspondence with immunostaining.

Interestingly, there was significantly elevated ^{18}F-GE180 signal in both the CNS and peripheral tissues (i.e., spleen and blood), indicating that TSPO PET might be useful for investigating inflammation throughout the whole body in the context of PD. Conversely, ^{64}Cu-TREM1 mAb may be more suitable for examining subtle alterations in innate immune activation in the CNS because of its increased signal-to-background ratio compared with ^{18}F-GE180, as demonstrated by brain autoradiography.

Our autoradiography findings were supported by gene expression data using tissue from the ipsilateral striatum. That is, we found that *TSPO* and *TREM1* were both significantly upregulated in ipsilateral striatum of day 14 6-hydroxydopamine mice compared with saline mice and that there was a strong trend toward significant elevation of both genes in day 7 6-hydroxydopamine animals (*TSPO,* $P < 0.0598$, and *TREM1,* $P < 0.0776$). Importantly, the fold change in *TREM1* expression was nearly 30 times greater than for *TSPO,* reiterating that *TREM1* is likely a more sensitive biomarker for neuroinflammation in this model than is *TSPO*. Importantly, mouse and human RNA-sequencing data (https://www.brainrnaseq.org) (*41*) for TSPO and TREM1 show that cellular expression of these proteins is quite different. In mice, for example, basal TSPO levels are about 20-fold higher in resting microglia/macrophages than are TREM1 levels. Crucially, TREM1 is specifically expressed on myeloid lineage cells, whereas TSPO is found not only in microglia/macrophages but also in astrocytes or endothelial cells for both mice and humans (Supplemental Fig. 9). The stark differences in expression of these 2 genes, as well as differences in their basal levels, indicates that TREM1 PET might be a more sensitive and specific technique for monitoring aberrant innate immune activation in the CNS. Flow cytometry allowed further investigation of the molecular changes underpinning a positive TREM1 PET/autoradiography image. Our data suggest that peripheral infiltrating myeloid cells (e.g., neutrophils) are likely the predominant cell type expressing TREM1 in the ipsilateral brain tissue of 6-hydroxydopamine mice (and not brain-resident microglia); however, further studies are needed to confirm this possibility at different time points throughout the course of disease in this model. Images acquired using ^{18}F-GE180, on the other hand, most likely reflect a combination of TSPO-expressing microglia, macrophages, astrocytes, and endothelial cells, reinforcing the importance of understanding the cellular specificity of an imaging biomarker in a given context or disease when interpreting imaging data. Accordingly, our future studies will involve additional flow cytometry comparing TSPO- and TREM1-expressing cells in different tissues in this mouse model (and other PD-like models) in addition to immunohistochemistry or multiplexed methods of probing the expression and spatial distribution of TSPO and TREM1 in human postmortem PD versus healthy control brain tissue. Such studies will help to further parse out the various cell types that express TSPO or TREM1 in different contexts.

CONCLUSION

Here, we showed that both TSPO and TREM1 PET enabled detection of innate immune activation after selective dopaminergic degeneration in a rodent model of PD-like pathology; however, there were some key differences in the molecular information these techniques afforded. That is, our data provided definitive evidence of the high specificity and sensitivity of TREM1 PET for imaging peripheral CNS-infiltrating myeloid cells in the brain of mice injected with 6-hydroxydopamine, whereas TSPO PET provided information on a larger array of cell types in the CNS and may be more useful for detecting inflammatory changes in both the brain and peripheral tissues of these mice, highlighting the potential of whole-body imaging using TSPO tracers. The current availability of TSPO PET (*42*) for clinical use allows for immediate testing of whole-body molecular imaging of PD patients. TREM1 PET, on the other hand, may help reveal unprecedented insights into the role of peripheral CNS-infiltrating myeloid cells in the pathogenesis of PD, both in rodent models and in patients after successful translation.

DISCLOSURE

This work was generously supported by the Smart Foundation. Michelle James is a cofounder and board member of Willow Neuroscience. No other potential conflict of interest relevant to this article was reported.

ACKNOWLEDGMENTS

We are very grateful to Dr. Jason Thanh Lee from the Sci^3 small-animal imaging facility at Stanford University for his continual support and gracious assistance with PET/CT imaging. We also want to thank Theresa McLaughlin at the Vincent Coates Foundation Mass Spectrometry Laboratory and Stanford University Mass Spectrometry (SUMS) for her help with the liquid chromatography–mass spectrometry data. We are truly grateful to Dr. Emily M. Deal for her assistance with editing and assembling the manuscript. Lastly, figures were assembled/created with BioRender.com.

KEY POINTS

QUESTION: Can ^{18}F-GE-180 (TSPO PET) and ^{64}Cu-TREM1 mAb (TREM1 PET) detect different types of cells involved in innate immune activation in a mouse model of PD-like pathology?

PERTINENT FINDINGS: TSPO and TREM1 PET enabled visualization and monitoring of innate immune cell activation and infiltration in a mouse model of PD-like pathology, with significant tracer binding observed in animals with dopaminergic cell degeneration compared with controls. In vivo findings were corroborated by ex vivo autoradiography, flow cytometry, and immunohistochemistry.

IMPLICATIONS FOR PATIENT CARE: The future translation of ^{64}Cu-TREM1 mAb and immediate availability of multiple TSPO PET radiotracers for clinical research could permit noninvasive biomarker-driven disease staging and monitoring of the inflammatory component of PD while facilitating the development and real-time assessment of novel immunomodulatory therapeutics for this disease.

REFERENCES

1. Holmqvist S, Chutna O, Bousset L, et al. Direct evidence of Parkinson pathology spread from the gastrointestinal tract to the brain in rats. *Acta Neuropathol (Berl).* 2014;128:805–820.
2. Blanz J, Saftig P. Parkinson's disease: acid-glucocerebrosidase activity and alpha-synuclein clearance. *J Neurochem.* 2016;139(suppl 1):198–215.
3. Moore DJ, West AB, Dawson VL, Dawson TM. Molecular pathophysiology of Parkinson's disease. *Annu Rev Neurosci.* 2005;28:57–87.
4. Grozdanov V, Bousset L, Hoffmeister M, et al. Increased immune activation by pathologic alpha-synuclein in Parkinson's disease. *Ann Neurol.* 2019;86:593–606.
5. Tan EK, Chao YX, West A, Chan LL, Poewe W, Jankovic J. Parkinson disease and the immune system: associations, mechanisms and therapeutics. *Nat Rev Neurol.* 2020;16:303–318.
6. Kam TI, Hinkle JT, Dawson TM, Dawson VL. Microglia and astrocyte dysfunction in Parkinson's disease. *Neurobiol Dis.* 2020;144:105028.
7. McGeer PL, Itagaki S, Boyes BE, McGeer EG. Reactive microglia are positive for HLA-DR in the substantia nigra of Parkinson's and Alzheimer's disease brains. *Neurology.* 1988;38:1285–1291.
8. Liu B, Gao HM, Hong JS. Parkinson's disease and exposure to infectious agents and pesticides and the occurrence of brain injuries: role of neuroinflammation. *Environ Health Perspect.* 2003;111:1065–1073.
9. Mogi M, Harada M, Riederer P, Narabayashi H, Fujita K, Nagatsu T. Tumor necrosis factor-α (TNF-α) increases both in the brain and in the cerebrospinal fluid from parkinsonian patients. *Neurosci Lett.* 1994;165:208–210.
10. Mogi M, Harada M, Kondo T, et al. Interleukin-1β, interleukin-6, epidermal growth factor and transforming growth factor-α are elevated in the brain from parkinsonian patients. *Neurosci Lett.* 1994;180:147–150.
11. Boka G, Anglade P, Wallach D, Javoy-Agid F, Agid Y, Hirsch EC. Immunocytochemical analysis of tumor necrosis factor and its receptors in Parkinson's disease. *Neurosci Lett.* 1994;172:151–154.
12. Mogi M, Kondo T, Mizuno Y, Nagatsu T. p53 protein, interferon-gamma, and NF-κB levels are elevated in the parkinsonian brain. *Neurosci Lett.* 2007;414:94–97.
13. Hirsch EC, Hunot S. Neuroinflammation in Parkinson's disease: a target for neuroprotection? *Lancet Neurol.* 2009;8:382–397.
14. Tansey MG, McCoy MK, Frank-Cannon TC. Neuroinflammatory mechanisms in Parkinson's disease: potential environmental triggers, pathways, and targets for early therapeutic intervention. *Exp Neurol.* 2007;208:1–25.
15. McGeer PL, Itagaki S, Akiyama H, McGreer EG. Rate of cell death in parkinsonism indicates active neuropathological process. *Ann Neurol.* 1988;24:574–576.
16. Brendel M, Probst F, Jaworska A, et al. Glial activation and glucose metabolism in a transgenic amyloid mouse model: a triple-tracer PET study. *J Nucl Med.* 2016;57:954–960.
17. Liu B, Le KX, Park MA, et al. In vivo detection of age- and disease-related increases in neuroinflammation by ^{18}F-GE180 TSPO microPET imaging in wild-type and Alzheimer's transgenic mice. *J Neurosci.* 2015;35:15716–15730.
18. Chaney A, Cropper HC, Johnson EM, et al. ^{11}C-DPA-713 versus ^{18}F-GE-180: a preclinical comparison of translocator protein 18 kDa PET tracers to visualize acute and chronic neuroinflammation in a mouse model of ischemic stroke. *J Nucl Med.* 2019;60:122–128.
19. James ML, Belichenko NP, Shuhendler AJ, et al. [^{18}F]GE-180 PET detects reduced microglia activation after LM11A-31 therapy in a mouse model of Alzheimer's disease. *Theranostics.* 2017;7:1422–1436.
20. Boutin H, Murray K, Pradillo J, et al. ^{18}F-GE-180: a novel TSPO radiotracer compared to ^{11}C-R-PK11195 in a preclinical model of stroke. *Eur J Nucl Med Mol Imaging.* 2015;42:503–511.
21. Sridharan S, Lepelletier FX, Trigg W, et al. Comparative evaluation of three TSPO PET radiotracers in a LPS-induced model of mild neuroinflammation in rats. *Mol Imaging Biol.* 2017;19:77–89.
22. Wadsworth H, Jones PA, Chau WF, et al. [^{18}F]GE-180: a novel fluorine-18 labelled PET tracer for imaging translocator protein 18 kDa (TSPO). *Bioorg Med Chem Lett.* 2012;22:1308–1313.
23. Werry EL, Bright FM, Piguet O, et al. Recent developments in TSPO PET imaging as a biomarker of neuroinflammation in neurodegenerative disorders. *Int J Mol Sci.* 2019;20:3161.
24. Bouchon A, Dietrich J, Colonna M. Cutting edge: inflammatory responses can be triggered by TREM-1, a novel receptor expressed on neutrophils and monocytes. *J Immunol.* 2000;164:4991–4995.
25. Liu Q, Johnson EM, Lam RK, et al. Peripheral TREM1 responses to brain and intestinal immunogens amplify stroke severity. *Nat Immunol.* 2019;20:1023–1034.
26. Chaney A, Cropper H, Johnson E, Stevens M, James M. Imaging the invaders: TREM1 as a novel PET imaging biomarker of peripheral infiltrating myeloid cells

and potential therapeutic target in multiple sclerosis [abstract]. *J Nucl Med.* 2019; 60(suppl 1):1506b.
27. Chaney A, Wilson E, Jain P, et al. TREM1-PET imaging of pro-inflammatory myeloid cells distinguishes active disease from remission in multiple sclerosis [abstract]. *J Nucl Med.* 2020;61(suppl 1):199.
28. Bové J, Prou D, Perier C, Przedborski S. Toxin-induced models of Parkinson's disease. *NeuroRx.* 2005;2:484–494.
29. Weber B, Schuster S, Zysset D, et al. TREM-1 deficiency can attenuate disease severity without affecting pathogen clearance. *PLoS Pathog.* 2014;10:e1003900.
30. Park SE, Song KI, Kim H, Chung S, Youn I. Graded 6-OHDA-induced dopamine depletion in the nigrostriatal pathway evokes progressive pathological neuronal activities in the subthalamic nucleus of a hemi-parkinsonian mouse. *Behav Brain Res.* 2018;344:42–47.
31. Boix J, Padel T, Paul G. A partial lesion model of Parkinson's disease in mice: characterization of a 6-OHDA-induced medial forebrain bundle lesion. *Behav Brain Res.* 2015;284:196–206.
32. Verel I, Visser GWM, Boellaard R, Stigter-van Walsum M, Snow GB, van Dongen GA. ^{89}Zr immuno-PET: comprehensive procedures for the production of ^{89}Zr-labeled monoclonal antibodies. *J Nucl Med.* 2003;44:1271–1281.
33. Cree BAC, Bennett JL, Kim HJ, et al. Inebilizumab for the treatment of neuromyelitis optica spectrum disorder (N-MOmentum): a double-blind, randomised placebo-controlled phase 2/3 trial. *Lancet.* 2019;394:1352–1363.
34. Hartung DM. Economics and cost-effectiveness of multiple sclerosis therapies in the USA. *Neurotherapeutics.* 2017;14:1018–1026.
35. Chaney AM, Johnson EM, Cropper HC, James ML. PET imaging of neuroinflammation using [^{11}C]DPA-713 in a mouse model of ischemic stroke. *J Vis Exp.* 2018; 136:57243.
36. Cropper HC, Johnson EM, Haight ES, et al. Longitudinal translocator protein-18 kDa-positron emission tomography imaging of peripheral and central myeloid cells in a mouse model of complex regional pain syndrome. *Pain.* 2019; 160:2136–2148.
37. Nicol LS, Dawes JM, La Russa F, et al. The role of G-protein receptor 84 in experimental neuropathic pain. *J Neurosci.* 2015;35:8959–8969.
38. Cicchetti F, Brownell AL, Williams K, Chen YI, Livni E, Isacson O. Neuroinflammation of the nigrostriatal pathway during progressive 6-OHDA dopamine degeneration in rats monitored by immunohistochemistry and PET imaging. *Eur J Neurosci.* 2002;15:991–998.
39. Tu LN, Zhao AH, Hussein M, Stocco DM, Selvaraj V. Translocator protein (TSPO) affects mitochondrial fatty acid oxidation in steroidogenic cells. *Endocrinology.* 2016;157:1110–1121.
40. Joshi N, Singh S. Updates on immunity and inflammation in Parkinson disease pathology. *J Neurosci Res.* 2018;96:379–390.
41. Zhang Y, Chen K, Sloan SA, et al. An RNA-sequencing transcriptome and splicing database of glia, neurons, and vascular cells of the cerebral cortex. *J Neurosci.* 2014;34:11929–11947.
42. Endres CJ, Pomper MG, James M, et al. Initial evaluation of ^{11}C-DPA-713, a novel TSPO PET ligand, in humans. *J Nucl Med.* 2009;50:1276–1282.